Geometry and dynamics for hierarchical regular networks

2008 J. Phys. A: Math. Theor. 41 335003

(http://iopscience.iop.org/1751-8121/41/33/335003)

IOP PUBLISHING JOURNAL OF PHYSICS A: MATHEMATICAL AND THEORETICAL

J. Phys. A: Math. Theor. **41** (2008) 335003 (25pp) doi:10.1088/1751-8113/41/33/335003

Geometry and dynamics for hierarchical regular networks

Stefan Boettcher[1], **Bruno Goncalves**[2] **and Julian Azaret**

Department of Physics, Emory University, Atlanta, GA 30322, USA

Received 20 May 2008
Published 17 July 2008
Online at stacks.iop.org/JPhysA/41/335003

Abstract

The recently introduced hierarchical regular networks HN3 and HN4 are analyzed in detail. We use renormalization group arguments to show that HN3, a 3-regular planar graph, has a diameter growing as $\sqrt{N}$ with the system size, and random walks on HN3 exhibit super-diffusion with an anomalous exponent $d_w = 2 - \log_2(\phi) \approx 1.306$, where $\phi = (\sqrt{5}+1)/2 = 1.618\ldots$ is the 'golden ratio.' In contrast, HN4, a non-planar 4-regular graph, has a diameter that grows slower than any power of N, yet, faster than any power of $\ln N$. In an annealed approximation we can show that diffusive transport on HN4 occurs ballistically ($d_w = 1$). Walkers on both graphs possess a first-return probability with a power law tail characterized by an exponent $\mu = 2 - 1/d_w$. It is shown explicitly that recurrence properties on HN3 depend on the starting site.

PACS number: 05.40.−a

(Some figures in this article are in colour only in the electronic version)

1. Introduction

Networks with a sufficiently intricate structure to exhibit not-trivial properties for statistical models but sufficiently simple to reveal analytical insights are few and far between. Familiar examples are random graphs [1, 2], the hierarchical lattices [3] originating in the Migdal–Kadanoff bond-moving scheme [4, 5], fractal lattices [6] or scale-free networks [7–9]. Scale-free networks and random graphs can elucidate mean-field properties only, whereas hierarchical lattices often provide excellent results for complex statistical models in low dimensions [10] but do not possess a mean-field limit. Fractal lattices provide tantalizing access to dynamical systems in non-integer dimensions but cannot be tuned across dimensions. From the perspective of statistical physics, it could be desirable to have a network that combines

[1] http://www.physics.emory.edu/faculty/boettcher/.
[2] http://www.bgoncalves.com/index.shtml.

solvability for low-dimensional systems with mean-field properties in such a way that one could interpolate between either extreme.

We have recently introduced a set of networks that overlay a lattice backbone with regular long-range links [11, 12], similar to small-world networks [13] but hierarchical and without randomness. These networks have a recursive construction but retain a fixed, regular degree. The hierarchical sequence of long-distance links occur in a pattern reminiscent of the tower-of-Hanoi sequence [12]. Therefore, we have dubbed them 'Hanoi-Networks' and abbreviated them as HN3 and HN4, since one is 3-regular and the other 4-regular. While almost identical, both types of networks lead to very distinct behaviors, as revealed by our studies here. Future work will focus on detailed studies of Ising models on these networks. In [11], we have shown already that spin models on HN4 have the desired properties mentioned above. Here, we analyze in great detail diffusive transport on these networks, for which especially HN3 proves to possess a rich behavior.

The paper is structured as follows. In the following section, we introduce the networks and discuss various key design aspects. In section 3, we explore geometric aspects of the networks such as their diameter. Section 4 contains our analysis of random walks on both networks, starting with a review of the dynamic renormalization group in the context of a simple one-dimensional random walk which facilitates an efficient discussion of the equivalent but far more involved calculation for HN3. Unfortunately, the same approach does not seem to apply to HN4, so we conclude the section with a derivation of a moment-generating equation in Fourier space for walks on HN4 directly from the master equation and an annealed approximation. We conclude this paper in section 5, indicating various future projects that can be developed from the work presented here.

2. Network design

Both networks that we are discussing in this paper consist of a simple geometric backbone, a one-dimensional line of $N = 2^k$ sites, either infinite ($-2^k \leqslant n \leqslant 2^k, k \to \infty$), semi-infinite ($0 \leqslant n \leqslant 2^k, k \to \infty$) or closed into a ring. Each site on the one-dimensional lattice backbone is connected to its nearest neighbor. (In general, the following procedure also works with a higher-dimensional lattice.)

To generate the small-world hierarchy in these graphs, consider parameterizing any integer n (except for zero) *uniquely* in terms of two other integers $(i, j), i \geqslant 0$, via

$$n = 2^i(2j + 1). \tag{1}$$

Here, i denotes the level in the hierarchy whereas j labels consecutive sites within each hierarchy. For instance, $i = 0$ refers to all odd integers, $i = 1$ to all integers once divisible by 2 (i.e., 2, 6, 10, ...) and so on. In these networks, aside from the backbone, each site is also connected with (one or both) of its nearest neighbors *within* the hierarchy. For example, we obtain the 3-regular network HN3 (best done on a semi-infinite line) by connecting first all nearest neighbors along the backbone, but in addition also 1 to 3, 5 to 7, 9 to 11, etc, for $i = 0$, next 2 to 6, 10 to 14, etc, for $i = 1$, and 4 to 12, 20 to 28, etc, for $i = 2$ and so on, as depicted in figure 1. Correspondingly, HN4 is obtained in the same manner, but connecting to *both* neighbors in the hierarchy, i.e., 1 to 3, 3 to 5, 5 to 7, etc, for $i = 0$, 2 to 6, 6 to 10, etc, for $i = 1$ and so forth. For this network it is clearly preferable to extend the line to $-\infty < n < \infty$ and also connect -1 to 1, -2 to 2, etc, as well as all negative integers in the above pattern, see figure 2. The site with index zero, not being covered by equation (1), is clearly a special place, either on the boundary of the HN3 or in the center of the HN4. It is easy to generalize these graphs, for instance, by putting the structure on a ring with periodic

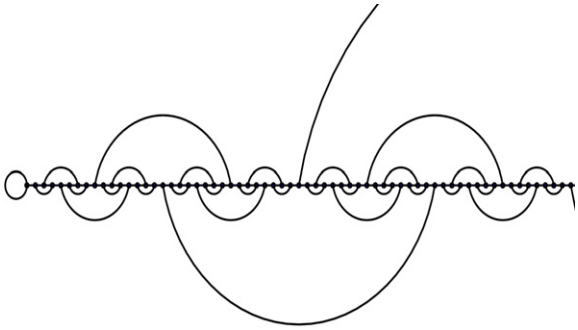

Figure 1. Depiction of HN3 on a semi-infinite line. The leftmost site here is $n = 0$, which requires special treatment. The entire network can be made 3-regular with a self-loop at $n = 0$. Note that HN3 is planar.

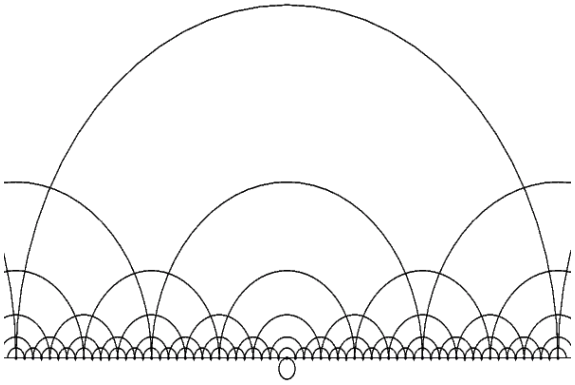

Figure 2. Depiction of HN4 on an infinite line. The center site is $n = 0$, which requires special treatment. The entire network becomes 4-regular with a self-loop at $n = 0$. Note that HN4 is non-planar.

boundary conditions, which may require special treatment of the highest level in the hierarchy on finite rings.

Random walks on these networks have fascinating properties due to their fractal nature and their long-range links as shown, for instance, in figure 3.

3. Network geometry

3.1. Distance measure on HN3

For HN3, it is simple to determine geometric properties, for instance, its diameter d, which is the longest of the shortest paths between any two sites, to wit, on a finite graph of size $N = N_k = 2^k$ for $k \to \infty$. Clearly, d in this case would be the end-to-end distance between sites $n = 0$ and $n = N$ with the smallest number of hops. Using a sequence of networks for $k = 2, 4, 6, \ldots$, the diameter-path looks like a Koch curve, see figure 4. We can define the path Π_k as a sequence of jumps reaching from one end of the $N = 2^k$-long graph to the other

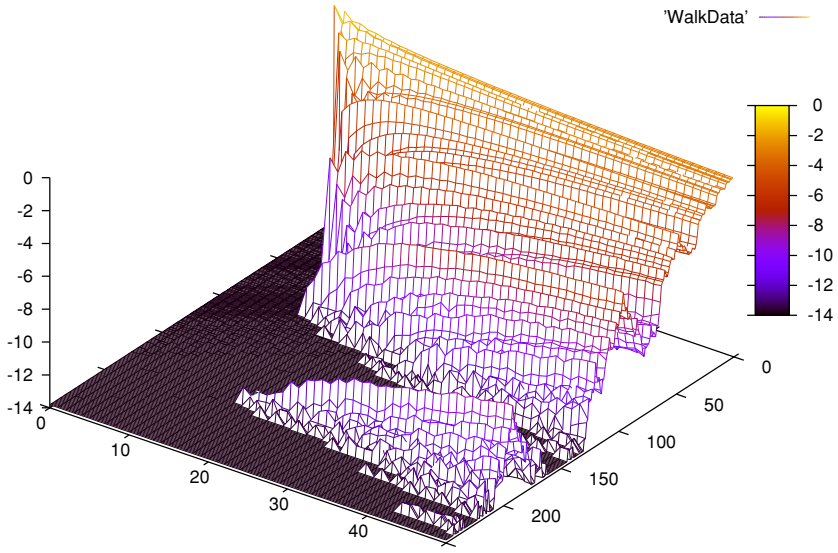

Figure 3. Plot of the probability $P_{l,t}$ of a random walker to reside at a site l at time t after starting at the origin $l = 0$ obtained by numerical simulations on HN3. The scale of the vertical axis refers to $\ln P_{l,t}$ to increase the visibility. Note the highly non-homogeneous evolution, which is tied to fractal distance-dependence also apparent in figure 5 due to the hierarchy of long-range links. Those links allow for walkers to appear suddenly at certain sites such as $l = 3 \times 2^i = 6, 12, 24, 48, 96, 192, \ldots$ long before ordinary diffusion along the backbone itself would provide for. Those onset-points for the most rapidly progressing walker should follow an envelope function that is linear ('ballistic') in a spacetime plot, as walkers diffuse ordinarily with hopping distance, $d \sim \sqrt{t}$, but by equation (4), $d \sim \sqrt{l}$, hence, $l \sim t$. Average walkers progress slower than ballistic, though, but still faster than diffusion.

via

$$\begin{aligned} &\Pi_0 = 1, \\ &\Pi_2 = 1 - 2 - 1 = \Pi_0 - 2 - \Pi_0, \\ &\Pi_4 = 1 - 2 - 1 - 8 - 1 - 2 - 1 = \Pi_2 - 8 - \Pi_2, \\ &\ldots, \\ &\Pi_{k+2} = \Pi_k - 2^{k+1} - \Pi_k, \end{aligned} \tag{2}$$

with an obvious notation of using '$-$' to string together a sequence of ever more complex moves. (While somewhat redundant here, introducing this notation will prove useful for HN4 below.) Hence, the length d_k of each path Π_k is given by

$$d_{k+2} = 2d_k + 1 \qquad \text{for} \quad N_{k+2} = 4N_k, \tag{3}$$

thus,

$$d \sim \sqrt{N}. \tag{4}$$

This property is demonstrated also in figure 5. In some ways, this property is reminiscent of a square lattice consisting of N lattice sites. The diameter (=diagonal) of this square is also $\sim\sqrt{N}$. In this sense, presuming that each link corresponds to a unit distance, HN3 is a fractal lattice of dimension 2, i.e., filling the plane. As shown in figure 6, we also find that the number of sites that can be reached from a given site grows quadratically with the number of jumps allowed. It should be noted, though, that we are employing the one-dimensional

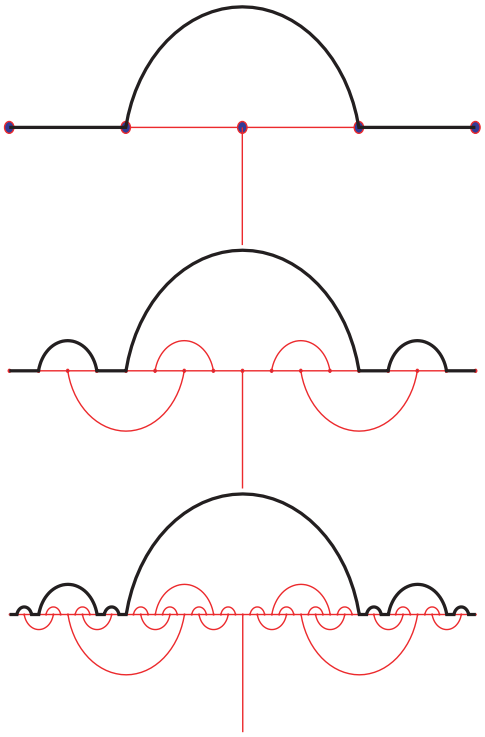

Figure 4. Sequence of shortest end-to-end paths (=diameter, thick black lines) for HN3 of size $N = 2^k, k = 2, 4, 8$. (Note that every second step in the hierarchical development has been omitted. At level $k = 3, 5, \ldots$ the shortest path is the same as at $k - 1$, except each linear segment counts for two steps.) Whenever the system size N increases by a factor of 4, the diameter d increases by a factor of $\sim$2, leading to equation (4).

lattice backbone as our metric to measure distances in the random walks in section 4, which enforces a trivial fractal dimension of $d_f = 1$. We conclude that, while interesting in its own right, HN3 is far from any mean-field behavior for which we would expect typical distances to depend only on (some power of) $\ln N$.

3.2. Distance measure on HN4

The situation is more interesting for the HN4. Using the notation from equation (2), we have

$$\begin{aligned}
\Pi_0 &= 1,\\
\Pi_1 &= 1 - 1,\\
\Pi_2 &= 1 - 2 - 1 = \Pi_0 - 2 - \Pi_0,\\
\Pi_3 &= 1 - 2 - 2 - 2 - 1 = \Pi_0 - 3 \times 2 - \Pi_0,\\
\Pi_4 &= 1 - 1 - 4 - 4 - 4 - 1 - 1\\
&= \Pi_1 - 3 \times 4 - \Pi_1,\\
\Pi_5 &= 1 - 2 - 1 - 8 - 8 - 8 - 1 - 2 - 1\\
&= \Pi_2 - 3 \times 8 - \Pi_2,\\
\Pi_6 &= 1 - 2 - 1 - 7 \times 8 - 1 - 2 - 1\\
&= \Pi_2 - 7 \times 8 - \Pi_2
\end{aligned} \tag{5}$$

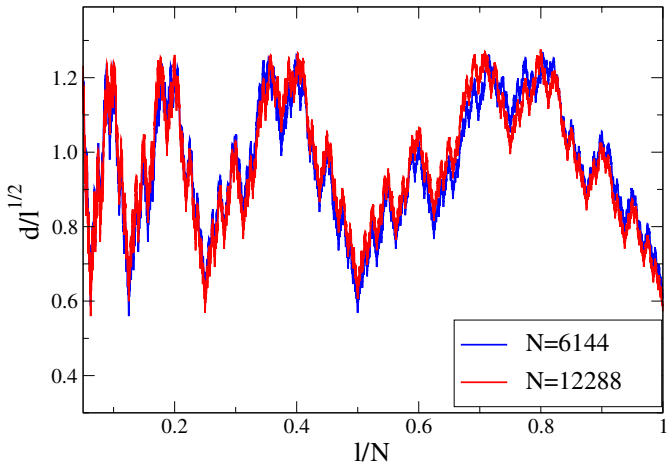

Figure 5. Plot of the shortest path length between the origin of HN3 and the lth site on two networks of extend $N = 3 \times 2^{11}$ and $N = 3 \times 2^{12}$. In both sets of data, we plot the path-distance relative to the root of the separation between site l and the origin ($l = 0$) along the linear backbone. Then, all rescaled distances fluctuate around a constant mean. Those fluctuations are very fractal, their self-similarity becoming apparent when super-imposing the data for both sizes N on a relative distance scale with l/N.

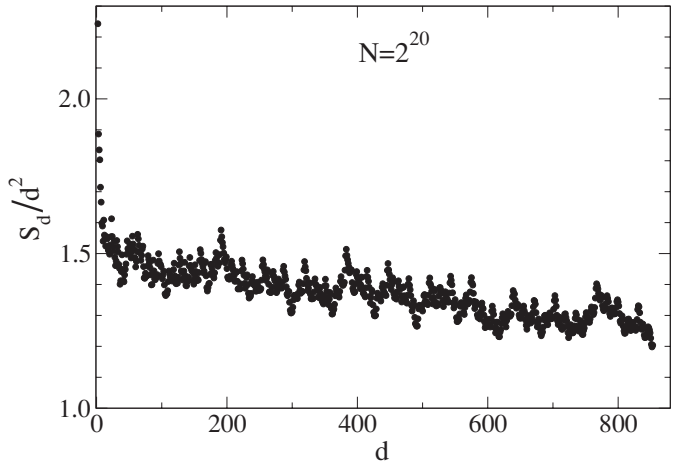

Figure 6. Plot of the number of sites (or 'neighborhood') S_d that can be reached from a given site within less than d jumps on HN3. Averaged over many starting sites, S_d/d^2 slowly converges to a constant, demonstrating that S_d grows quadratically with d. Note that some features due to the hierarchical structure remain even after averaging over sites, such as the peaks at $d = 192$, 384, 768, etc.

and so on. Due to degeneracies at each level (which we have not listed), one has to proceed to many more levels in the hierarchy to discern the relevant pattern. In fact, any pattern evolves for an increasing number of levels before it gets taken over by a new one, with two patterns

creating degeneracies at the crossover. Finally, we get (setting the degeneracies aside)

$$\Pi_k = \begin{cases} \Pi_{k-2} - 1 \times 2^{k-1} - \Pi_{k-2}, & (k = 2), \\ \Pi_{k-3} - 3 \times 2^{k-2} - \Pi_{k-3}, & (2 < k \leqslant 5), \\ \Pi_{k-4} - 7 \times 2^{k-3} - \Pi_{k-4}, & (5 < k \leqslant 9), \\ \Pi_{k-5} - 15 \times 2^{k-4} - \Pi_{k-5}, & (9 < k \leqslant 14), \\ \ldots \end{cases} \tag{6}$$

and so on.

Note that the paths here do *not* search out the longest possible jump, as in equation (2). Instead, the paths reach quickly to some intermediate level and follow *consecutive* jumps at that level before trailing off in the end. As we will see repeatedly, this is the main distinguishing feature discriminating between HN3 and HN4: once a level is reached in the HN4, the entire graph can be traversed at *that* level, while in the HN3 any transport *must* climb down to lower levels (or merely jump back on that level), see figures 1–2.

Corresponding to equation (6), we obtain for the end-to-end shortest paths (=diameters d_k)

$$d_k = \begin{cases} 2d_0 + 1, & (k = 2), \\ 2d_{k-3} + 3, & (2 < k \leqslant 5), \\ 2d_{k-4} + 7, & (5 < k \leqslant 9), \\ \ldots, \end{cases} \tag{7}$$

which we can generalize into a single statement introducing a 'generation' index $g \geqslant 2$,

$$d_k^g = 2d_{k-g}^{g-1} + (2^{g-1} - 1), \qquad (l_{g-1} < k \leqslant l_g), \tag{8}$$

defining $l_1 = 1$, where in general

$$l_g = l_{g-1} + g, \qquad l_2 = 2, \tag{9}$$

demarcates the crossover point between the generations, see figure 7. Equation (9) easily yields

$$l_g = \tfrac{1}{2} g(g+1) - 1 \qquad (g \geqslant 2). \tag{10}$$

To obtain the asymptotic behavior for d_k, instead of solving equation (8) for all k, we note that exactly on the crossover points $k = l_g$ (i.e., $k - g = l_{g-1}$) we have

$$d_{l_g}^g = 2d_{l_{g-1}}^{g-1} + (2^{g-1} - 1). \tag{11}$$

Defining $e_g = 2^g d_{l_g}^g$, we get

$$e_g = e_{g-1} + \tfrac{1}{2} - 2^{-g}, \tag{12}$$

which is easily summed up to give

$$d_{l_g}^g = (g-1)2^{g-1} + 1. \tag{13}$$

Remembering that $k = l_g$ and, from equation (10), that $g \sim \sqrt{2l_g} \sim \sqrt{2k} \sim \sqrt{\log_2 N^2}$, we finally get

$$d_k \sim \tfrac{1}{2}\sqrt{\log_2 N^2}\, 2^{\sqrt{\log_2 N^2}} \qquad (N \to \infty) \tag{14}$$

for the diameter of the HN4. As we would expect that the diameter (or rather, the average of shortest paths) in a small-world graph should behave as $d \sim \log N$, it is instructive to rewrite

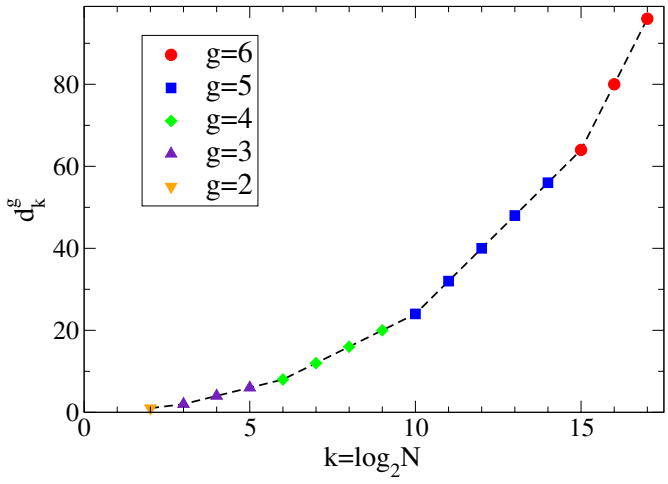

Figure 7. Plot of the shortest end-to-end path length for HN4 networks of increasing backbone sizes $N = 2^k$, obtained by simulation. Note the piecewise-linear shape of the graph, which is reflected in equation (7), for example. In turn, equation (11) concerns only the 'bends' between each consecutive linear segment g.

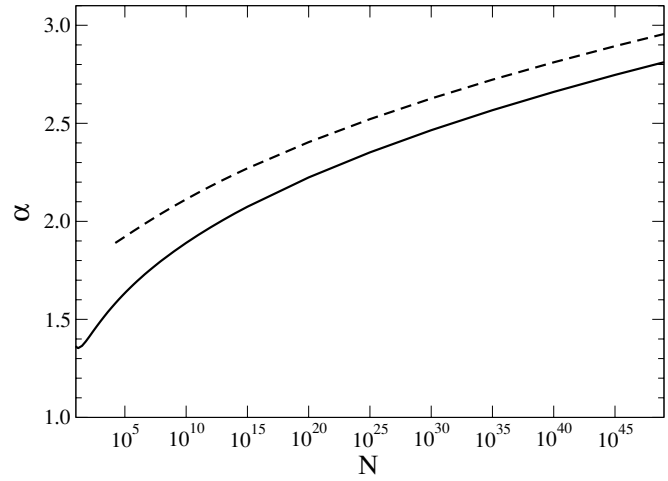

Figure 8. Plot of the system-size dependence of the exponent $\alpha = \alpha(N)$ defined in equation (15). The solid curve is the exact value based on equation (13), and the dashed curve is the asymptotic approximation also given in equation (15). This approximation is always an upper bound. Note that $\alpha(N)$ barely varies within a factor of 2 over 50 orders of magnitude.

equation (14) as

$$d_k \sim (\log_2 N)^\alpha \qquad \text{with} \qquad \alpha \sim \frac{\sqrt{2\log_2 N}}{\log_2 \log_2 N} + \frac{1}{2}. \tag{15}$$

Technically, of course, α diverges with N and the diameter grows faster than any power of $\log_2 N$ but less than any however-small power of N, unlike equation (4). In reality, though, α varies only very slowly with N, ranging merely from $\alpha \approx 1.5$ to 3 over 50 decades, see figure 8.

4. Random walks

In the following we will study random walks on HN3 and HN4. For simplicity, we have focused in our simulations only on two elementary observables, the mean displacement with time, $\langle |l| \rangle \sim t^{1/d_w}$, and the first-return time distribution $Q(\Delta t) \sim \Delta t^{-\mu}$. All walks are controlled by one parameter, p, which determines the probability of a walker to step off the lattice into the direction of a long-range jump. In particular, on HN3 a walker steps off the lattice with probability p and jumps either to the left or right neighbor with probability $(1-p)/2$, whereas on HN4 long-range jumps to either the left or right occur with probability $p/2$ instead. In both cases, we should return to a simple one-dimensional nearest-neighbor walk for $p \to 0$, where $d_w = 2$ and $\mu = 3/2$, although we would expect that limit to be singular. Here, we only consider uniform values of p, independent of the sites (or level of hierarchy). With a bit more algebra, the following considerations could be extended to values that for each site depend on the level of hierarchy, $p = p(i)$, for instance.

4.1. Renormalization group for random walks

Here, we analyze the spatio-temporal rescaling of simple random walks with nearest-neighbor jumps along the available links using the renormalization group. First, we review the method using as a simple example the well-known one-dimensional walk. Walks on such a graph obey simple diffusion, $d_w = 2$, which implies that each rescaling of space entails a rescaling of time according to

$$N \to N' = 2N \qquad T \to T' = 2^{d_w} T = 4T. \tag{16}$$

This is synonymous with the asymptotic form with the mean-square displacement

$$\langle |l| \rangle \sim t^{1/d_w}, \tag{17}$$

which defines the anomalous dimension of the walk in terms of the exponent d_w. While the result for the one-dimensional walk can be easily obtained with much simpler means, it serves as a pedagogical example of calculating first-passage and first-return times using RG on more complex structures. Later on, reference to this presentation will allow us to avoid excessive algebra.

4.1.1. RG for the 1D random walk. As a pedagogical example, we present here the theory as it will be applied in section 4.1.2. We consider a biased random walk on a finite one-dimensional line. The master equations for such a random walk on a lattice of length $N = 2^{K+1}$ with reflecting boundaries are given by

$$\begin{aligned}
P_{0,t+1} &= pP_{1,t}, \\
P_{1,t+1} &= P_{0,t} + pP_{2,t}, \\
P_{l,t+1} &= (1-p)P_{l-1,t} + pP_{l+1,t} \qquad (2 \leqslant l \leqslant N-2), \\
P_{N-1,t+1} &= (1-p)P_{N-2,t} + P_{N,t}, \\
P_{N,t+1} &= (1-p)P_{N-1,t},
\end{aligned} \tag{18}$$

where $P_{l,t}$ denotes the probability of a walker to be at site l at time t, p is the probability expressing the biasing for left or right hops. Since we want to start the walks at time $t = 0$ at the origin $l = 0$, these equations have the initial condition

$$P_{l,0} = \delta_{l,0}. \tag{19}$$

To facilitate renormalization of this non-equilibrium process, we introduce a generating function

$$\tilde{P}_l(z) = \sum_{t=0}^{\infty} P_{l,t} z^t \tag{20}$$

for all $0 \leqslant l \leqslant N$. Incorporating the initial condition in equation (19), equations (18) transform into

$$\begin{aligned}
\tilde{P}_0 &= a\tilde{P}_1 + 1, \\
\tilde{P}_1 &= c\tilde{P}_0 + a\tilde{P}_2, \\
\tilde{P}_l &= b\tilde{P}_{l-1} + a\tilde{P}_{l+1} \qquad (2 \leqslant l \leqslant N-2), \\
\tilde{P}_{N-1} &= b\tilde{P}_{N-2} + d\tilde{P}_N, \\
\tilde{P}_N &= b\tilde{P}_{N-1},
\end{aligned} \tag{21}$$

where we have inserted generalized 'hopping rates' in preparation for the RG. Initially, at the $k = 0$th RG step, it is

$$a^{(0)} = pz, \qquad b^{(0)} = (1-p)z, \qquad c^{(0)} = z, \qquad d^{(0)} = z, \tag{22}$$

which provides a sufficient number of renormalizable parameters that are potentially required to consider special sites at both boundaries.

A single step of applying the RG consists of solving equations (21) for $\tilde{P}_l$ with odd values of l (which is trivial here, as they are already expressed explicitly in terms of even ones) and eliminating them from the equations for the even l. After that elimination, we can rewrite the equations for even l as

$$\begin{aligned}
\tilde{P}_0 &= \frac{a^2}{1-ac}\tilde{P}_2 + \frac{1}{1-ac}, \\
\tilde{P}_2 &= \frac{bc}{1-2ab}\tilde{P}_0 + \frac{a^2}{1-2ab}\tilde{P}_4, \\
\tilde{P}_{2l} &= \frac{b^2}{1-2ab}\tilde{P}_{2l-2} + \frac{a^2}{1-2ab}\tilde{P}_{2l+2} \qquad \left(2 \leqslant l \leqslant \frac{N}{2} - 2\right), \\
\tilde{P}_{N-2} &= \frac{b^2}{1-2ab}\tilde{P}_{N-4} + \frac{ad}{1-2ab}\tilde{P}_N, \\
\tilde{P}_N &= \frac{b^2}{1-bd}\tilde{P}_{N-2}.
\end{aligned} \tag{23}$$

Comparing these equations with equations (21) allows us to extract the RG recursion equations. (Note that superscripts referring the kth RG step have been suppressed thus far in equations (21) and (23).)

Before we analyze the first return time at the boundary specifically, we can use the equation for bulk sites l in (23) to extract already the diffusion exponent d_w. A comparison of the respective coefficients in equations (21) and (23) yields

$$a^{(k+1)} = \frac{(a^{(k)})^2}{1-2a^{(k)}b^{(k)}}, \qquad b^{(k+1)} = \frac{(b^{(k)})^2}{1-2a^{(k)}b^{(k)}}. \tag{24}$$

These recursions converge for $k \to \infty$ toward fixed points (a^*, b^*) that characterize the dynamics in the infinite-time limit (which corresponds to the limit of $z \to 1^-$). The trivial fixed point $a^* = b^* = 0$ is unphysical, as it cannot be reached from the initial conditions in (22) for any choice of p (and $z = 1$). The physical fixed points are $(a^*, b^*) = (1, 0)$, which is reached for any bias $p > \frac{1}{2}$, or $(a^*, b^*) = (0, 1)$, reached for $p < \frac{1}{2}$; finally, $(a^*, b^*) = \left(\frac{1}{2}, \frac{1}{2}\right)$

can only be reached by entirely unbiased walks for $p = \frac{1}{2}$. To explore the behavior for large but finite times, we expand the RG recursions in (24) to first order in $\epsilon = 1 - z$ by writing for $y \in \{a, b\}$,

$$y^{(k)} \sim y^* + y_1^{(k)}\epsilon + \cdots. \tag{25}$$

Inserting the Ansatz in equation (25) into the recursions in equations (24), we obtain near the fixed point with $a^* = b^* = \frac{1}{2}$,

$$a_1^{(k+1)} = 3a_1^{(k)} + b_1^{(k)}, \qquad b_1^{(k+1)} = a_1^{(k)} + 3b_1^{(k)}, \tag{26}$$

with the result that

$$a_1^{(k)} = b_1^{(k)} \propto 4^k.$$

This implies that as space rescales by a factor of 2 (i.e., eliminating all odd-index sites), time rescales by a factor of 4, as indicated in equation (16) for an unbiased random walk, leading to $d_w = 2$. The same analysis for either of the biased fixed points yields that, for example, $a^{(k)} \equiv 0$ beyond any power of ϵ and, with the Ansatz $b^{(k)} \sim 1 + b_1^{(k)}\epsilon$ in equations (24), $b_1^{(k)} \propto 2^k$. Following the interpretation in equation (16), this would imply $d_w = 1$ and we find the familiar result that with the slightest bias, i.e., $p < \frac{1}{2}$ or $p > \frac{1}{2}$, the motion at large length and time scales is dominated by the constant-velocity drift upon reaching the bulk.

In this scenario of a bias, average first-return times are clearly system-size independent constants: a walker with a bias *toward* the origin $\left(p > \frac{1}{2}\right)$ will drift back recurrently after only small excursions; a walker with a bias *away* from the origin $\left(p < \frac{1}{2}\right)$ returns at most a finite number of times in short order until the drift eventually carries it away without further recurrence. In the following, we therefore focus exclusively on the unbiased case $p = \frac{1}{2}$. Then, we can equate $a = b$ at every step, to get from equation (24),

$$a^{(k+1)} = \frac{(a^{(k)})^2}{1 - 2(a^{(k)})^2}. \tag{27}$$

To derive the return-time behavior, we have to examine equations (23) more closely. Comparing coefficients also in the boundary terms lead to

$$c^{(k+1)} = \frac{a^{(k)}c^{(k)}}{1 - 2(a^{(k)})^2}, \qquad d^{(k+1)} = \frac{a^{(k)}d^{(k)}}{1 - 2(a^{(k)})^2}. \tag{28}$$

For large k, both $c^{(k)}$ and $d^{(k)}$ are entrained with $a^{(k)}$, and we obtain a consistent and closed set of relations for all coefficients in equations (21) and (23) by identifying $c = d = 2a$. Further renormalizing

$$\tilde{P}_l^{(k+1)} = [1 - 2(a^{(k)})^2]\tilde{P}_{2l}^{(k)} \tag{29}$$

ensures invariance of the constant term at the lower boundary that originated from the unit initial condition in equation (19).

After $k = K$ RG steps, the system has reduced to

$$\begin{aligned} \tilde{P}_0^{(K)} &= a^{(K)}\tilde{P}_1^{(K)} + 1, \\ \tilde{P}_1^{(K)} &= 2a^{(K)}\tilde{P}_0^{(K)} + 2a^{(K)}\tilde{P}_2^{(K)}, \\ \tilde{P}_2^{(K)} &= a^{(K)}\tilde{P}_1^{(K)}, \end{aligned} \tag{30}$$

which yields

$$\tilde{P}_0^{(K)} = \frac{1 - 2(a^{(K)})^2}{1 - 4(a^{(K)})^2}. \tag{31}$$

Using equation (29) in turn obtains

$$\tilde{P}_0^{(0)} = \frac{\tilde{P}_0^{(K)}}{\prod_{k=0}^{K-1}[1-2(a^{(k)})^2]} = \frac{1-2(a^{(K)})^2}{1-4(a^{(K)})^2} \prod_{k=0}^{K-1} \frac{1}{[1-2(a^{(k)})^2]}. \tag{32}$$

It is a well-known fact that the generating functions for being at the origin, $\tilde{P}_0^{(0)}$, and for the first-return probability to the same site, $\tilde{Q}_0$, satisfy the following simple relation [14]:

$$\tilde{Q}_{l=0} = 1 - \frac{1}{\tilde{P}_{l=0}^{(0)}}. \tag{33}$$

Note that a recurrent walk (with $\tilde{Q}_0 = 1$) requires that $\tilde{P}_0^{(0)}$ diverges at long times (i.e., $z \to 1^-$). In our one-dimensional walk here, it is $a^{(K)} \to a^* = \frac{1}{2}$, on behalf of which the denominator of $\tilde{P}_0^{(0)}$ in equation (32) has a zero, making the walk recurrent. In more detail, it is

$$\tilde{Q}_0 = 1 - \frac{1-4(a^{(K)})^2}{1-2(a^{(K)})^2} \prod_{k=0}^{K-1} [1-2(a^{(k)})^2]. \tag{34}$$

We intend to extract the exponent μ for the first-return probability distribution, which on a finite but large system of size $N \to \infty$ behaves as

$$Q_0(t) \sim t^{-\mu}\, \mathrm{e}^{-t/\tau_N} \qquad (t \to \infty), \tag{35}$$

where τ_N is a cut-off time scale that diverges in some form with N. As the physics of the return probabilities at any finite time should not change if the system size becomes infinite independently, it must be $\mu > 1$ for $Q_0(t)$ to remain normalizable. Based on that observation [14], we need to calculate the first two moments of $Q_0(t)$, corresponding to an expansion of $\tilde{Q}_0(z)$ to second order in $\epsilon = 1 - z$, to extract μ. Since $\mu > 1$, the normalization integral

$$\mathcal{N} \sim \int^{\infty} \mathrm{d}t\; t^{-\mu}\, \mathrm{e}^{-t/\tau_N} \sim O(1) \tag{36}$$

is dominated by its behavior for small t, which is irrelevant in detail except for the fact that it makes the integral become a constant independent of τ_N. If we further assume that $\mu < 2$, then for all $m \geqslant 1$, the integrals for those mth moments *do* diverge with τ_N,

$$\langle t^m \rangle_N \sim \frac{1}{\mathcal{N}} \int_0^{\infty} \mathrm{d}t\; t^{m-\mu}\, \mathrm{e}^{-t/\tau_N} \sim \tau_N^{m+1-\mu}. \tag{37}$$

From the ratio of $\langle t \rangle_N$ and $\langle t^2 \rangle_N$, we then obtain

$$\mu = \lim_{N\to\infty} 2 + \frac{1}{1 - \frac{\langle t^2 \rangle_N}{\langle t \rangle_N}}. \tag{38}$$

Luckily, due to the leading zero in $1 - 4(a^{(K)})^2$, any other factor in equation (34) only needs to be expanded to first order in ϵ. Extending the ansatz in equation (25) for $a^{(k)}$ to second order, we obtain here

$$a^{(K)} \sim \frac{1}{2} - \frac{1}{2} \times 4^K \epsilon + 5 \times 16^K \epsilon^2 + \cdots,$$
$$1 - 4(a^{(K)})^2 \sim 8 \times 4^K \epsilon + 116 \times 16^K \epsilon^2 + \cdots,$$
$$1 - 2(a^{(K)})^2 \sim \frac{1}{2} + 4 \times 4^K \epsilon + \cdots,$$

$$\prod_{k=0}^{K-1}[1-2(a^{(k)})^2] \sim \prod_{k=0}^{K-1}\left[\frac{1}{2}+4\times 4^k\epsilon+\cdots\right],$$
$$\sim 2^{-K}\left[1+8\epsilon\sum_{k=0}^{K-1}4^k+\cdots\right],$$
$$\sim 2^{-K}+\frac{8}{3}2^K\epsilon+\cdots.$$

Inserting these expressions into equation (34), we get

$$\tilde{Q}_0 \sim 1-16\times 2^K\epsilon+\tfrac{952}{3}\times 8^K\epsilon^2+\cdots. \tag{39}$$

The moments of $Q_0(t)$ are obtained via derivatives of $\tilde{Q}_0(z)$, i.e.,

$$\langle t^m\rangle = \left[z\frac{\mathrm{d}}{\mathrm{d}z}\right]^m \tilde{Q}_0(z)|_{z=1}. \tag{40}$$

Applied to equation (39), we calculate for the dominant asymptotics of the moments,

$$\langle t\rangle_K \sim 2^K \sim N, \qquad \langle t^2\rangle_K \sim 8^K \sim N^3,$$

which from equation (38) leads to the familiar first-return exponent of a one-dimensional walk,

$$\mu = \tfrac{3}{2}. \tag{41}$$

4.1.2. RG for the random walk on HN3. We follow the discussion for one-dimensional walkers above to model diffusion on HN3. The lesson of the previous section is that we only need to consider the bulk equations to extract the diffusion exponent d_w, and supplement with the calculation on the final system at the end of the $k = K$th step of the RG to obtain the first-return exponent for a system of size $N = 2^{K+1}$. We can section the line into segments centered around sites l with $i = 1$ in equation (1), i.e., $n = 2(2j+1)$. Such a site $l = n$ is surrounded by two sites of odd index, which are *mutually* linked. Furthermore, n is linked by a long-distance jump to a site also of type $i = 1$ at $l = n \pm 4$ in a neighboring segment, where the direction does not matter here. The sites $l = n \pm 2$, which are shared at the boundary between adjacent segments also have even index, but their value of $i \geqslant 2$ is undetermined and irrelevant for the immediate RG step, as they have a long-distance jump to some sites $l = m_\pm$ at least eight sites away.

In each segment in the bulk, the master equation reads

$$\begin{aligned}
P_{n+2,t+1} &= \frac{1-p}{2}[P_{n+3,t}+P_{n+1,t}]+pP_{m_+,t},\\
P_{n+1,t+1} &= \frac{1-p}{2}[P_{n+2,t}+P_{n,t}]+pP_{n-1,t},\\
P_{n,t+1} &= \frac{1-p}{2}[P_{n+1,t}+P_{n-1,t}]+pP_{n\pm4,t},\\
P_{n-1,t+1} &= \frac{1-p}{2}[P_{n,t}+P_{n-2,t}]+pP_{n+1,t},\\
P_{n-2,t+1} &= \frac{1-p}{2}[P_{n-1,t}+P_{n-3,t}]+pP_{m_-,t}.
\end{aligned} \tag{42}$$

Here, p is the (uniform) probability for a walker to take a long-range jump, whereas $(1-p)/2$ is the probability to jump either left or right toward a nearest-neighbor site along the backbone. Without restriction of generality, let us assume that we happened to let all walks start from a site within this segment. Note that, unlike for the 1D-walk above, there are *three* distinct

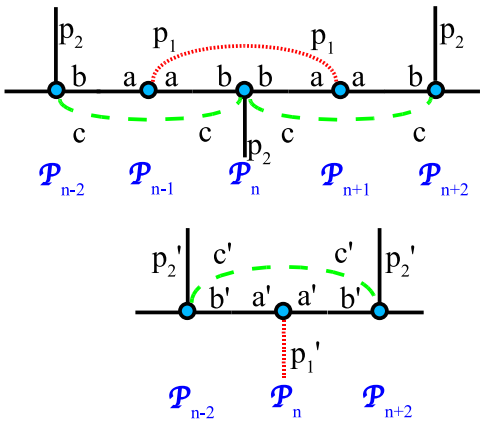

Figure 9. Depiction of the (exact) RG step for random walks on HN3. Hopping rates from one site to another along a link are labeled at the originating site. The RG step consists of tracing out odd-labeled variables $\tilde{P}_{n\pm1}$ in the top graph and expressing the renormalized rates (a', b', c', p_1', p_2') on the bottom in terms of the ones (a, b, c, p_1, p_2) from the top. The node $\tilde{P}_n$, bridged by a (dotted) link between $\tilde{P}_{n-1}$ and $\tilde{P}_{n+1}$, is special as it *must* have $n = 2(2j + 1)$ and is to be decimated at the following RG step, justifying the designation of p_1'. Note that the original graph in figure 1 does not have the green, dashed links with hopping rates (c, c'), which *emerge* during the RG recursion.

types of sites even in the bulk of this problem: $P_{n\pm2,t}$, $P_{n\pm1,t}$ and $P_{n,t}$. In principle, one could expect three distinct return-time behaviors as a result. We will demonstrate below that, indeed, different sites possess differences in their return-time behavior, depending on their level in the hierarchy, but all scale with the same exponent μ. Here, we choose to have the walk start on site $n - 2$ within this segment,

$$P_{l,0} = \delta_{l,n-2}. \tag{43}$$

Using the generating function in equation (20) on equations (42)–(43) yields

$$\begin{aligned}
\tilde{P}_{n+2} &= a[\tilde{P}_{n+3} + \tilde{P}_{n+1}] + c[\tilde{P}_{n+4} + \tilde{P}_n] + p_2\tilde{P}_{m_+},\\
\tilde{P}_{n+1} &= b[\tilde{P}_{n+2} + \tilde{P}_n] + p_1\tilde{P}_{n-1},\\
\tilde{P}_n &= a[\tilde{P}_{n+1} + \tilde{P}_{n-1}] + c[\tilde{P}_{n+2} + \tilde{P}_{n-2}] + p_2\tilde{P}_{n\pm4},\\
\tilde{P}_{n-1} &= b[\tilde{P}_n + \tilde{P}_{n-2}] + p_1\tilde{P}_{n+1},\\
\tilde{P}_{n-2} &= a[\tilde{P}_{n-1} + \tilde{P}_{n-3}] + c[\tilde{P}_n + \tilde{P}_{n-4}] + p_2\tilde{P}_{m_-} + 1,
\end{aligned} \tag{44}$$

where we have again absorbed the parameters p and z into general 'hoping rates', which are initially

$$a^{(0)} = b^{(0)} = \frac{z}{2}(1 - p), \qquad c^{(0)} = 0, \qquad p_1^{(0)} = p_2^{(0)} = zp. \tag{45}$$

Note that we have added new terms with a parameter c, which is zero initially. As figure 9 depicts, such links are not present in the original network HN3, but have to be taken into account during the RG process. In all, a surprising number of parameters, five in all, is required even for the most symmetric set of initial conditions to obtain a closed set of RG recursion equations. Unlike for the one-dimensional walk in equation (21), the parameters a and b here do not express a directional bias or drift along the backbone. Instead, they are necessary merely to distinguish between hops out of (currently) odd and even sites, respectively, as shown in figure 9.

The RG update step consists of eliminating from these five equations those two that refer to an odd index, $n \pm 1$. As a first step, adding the two relations referring to the indices $n \pm 1$, we obtain

$$\tilde{P}_{n+1} + \tilde{P}_{n-1} = \frac{b}{1-p_1}[\tilde{P}_{n+2} + 2\tilde{P}_n + \tilde{P}_{n-2}],$$

which allows us to eliminate any reference to odd sites $n \pm 1$ from the middle relation in (44). Furthermore, solving for $\tilde{P}_{n\pm1}$ explicitly,

$$\tilde{P}_{n\pm1} = \frac{b}{1-p_1^2}\tilde{P}_{n\pm2} + \frac{bp_1}{1-p_1^2}\tilde{P}_{n\mp2} + \frac{b}{1-p_1}\tilde{P}_n,$$

and inserting into the relations for $\tilde{P}_{n\pm2}$ in equation (44) result in

$$\begin{aligned}
\tilde{P}_{n+2} &= \frac{[ab + c(1-p_1)](1+p_1)}{1-p_1^2-2ab}[\tilde{P}_{n+4} + \tilde{P}_n] + \frac{abp_1}{1-p_1^2-2ab}[\tilde{P}_{n+6} + \tilde{P}_{n-2}] \\
&\quad + \frac{p_2(1-p_1^2)}{1-p_1^2-2ab}\tilde{P}_{m_+}, \\
\tilde{P}_n &= \frac{ab + c(1-p_1)}{1-p_1-2ab}[\tilde{P}_{n+2} + \tilde{P}_{n-2}] + \frac{p_2(1-p_1)}{1-p_1-2ab}\tilde{P}_{n\pm4}, \\
\tilde{P}_{n-2} &= \frac{[ab + c(1-p_1)](1+p_1)}{1-p_1^2-2ab}[\tilde{P}_n + \tilde{P}_{n-4}] + \frac{abp_1}{1-p_1^2-2ab}[\tilde{P}_{n+2} + \tilde{P}_{n-6}] \\
&\quad + \frac{p_2(1-p_1^2)}{1-p_1^2-2ab}\tilde{P}_{m_-} + \frac{1-p_1^2}{1-p_1^2-2ab}.
\end{aligned} \tag{46}$$

Given that n is only once divisible by 2, either $n-2$ or $n+2$ must be divisible by 2 at most twice, and we assume without restriction of generality that $n+2$ satisfies this description, whereas $n-2$ is divisible by a higher power of 2. (This also selects the upper sign in the index '$n \pm 4$'). As in equation (29), we now add the proper superscript for the kth RG step and obtain the renormalized generating functions at step $k+1$ as

$$\tilde{P}_l^{(k+1)} = \frac{1-\left(p_1^{(k)}\right)^2 - 2a^{(k)}b^{(k)}}{1-\left(p_1^{(k)}\right)^2}\tilde{P}_{2l}^{(k)}. \tag{47}$$

The proportionality factor in this relation arises from the necessity to preserve the unity of the initial condition, as in equation (29). Note that we would have obtained the *identical* factor, if we had chosen to start the walker from the central site n instead of $n+2$. Starting at a site like $n \pm 1$, in turn, would have provided a different factor,

$$\tilde{P}_l^{(k+1)} = \frac{1-p_1^{(k)} - 2a^{(k)}b^{(k)}}{1-p_1^{(k)}}\tilde{P}_{2l}^{(k)}, \tag{48}$$

potentially leading to a distinct return-time behavior. Yet, asymptotically for large times and distances both alternatives prove identical to sufficiently high order as to not affect the scaling discussed below.

Proceeding with the RG step, the role of the central site in the new segments is then specified via $\frac{n+2}{2} \to n$ such that $\tilde{P}_{n-2}^{(k)} \to \tilde{P}_{n-2}^{(k+1)}$, $\tilde{P}_n^{(k)} \to \tilde{P}_{n-1}^{(k+1)}$, $\tilde{P}_{n+2}^{(k)} \to \tilde{P}_n^{(k+1)}$, and correspondingly for the functions on the left-hand side of equations (46), which now reads

$$\begin{aligned}
\tilde{P}_n^{(k+1)} &= a^{(k+1)}\left[\tilde{P}_{n+1}^{(k+1)} + \tilde{P}_{n-1}^{(k+1)}\right] + c^{(k+1)}\left[\tilde{P}_{n+2}^{(k+1)} + \tilde{P}_{n-2}^{(k+1)}\right] + p_2^{(k+1)}\tilde{P}_{n\pm4}^{(k+1)}, \\
\tilde{P}_{n-1}^{(k+1)} &= b^{(k+1)}\left[\tilde{P}_n^{(k+1)} + \tilde{P}_{n-2}^{(k+1)}\right] + p_1^{(k+1)}\tilde{P}_{n+1}^{(k+1)}, \\
\tilde{P}_{n-2}^{(k+1)} &= a^{(k+1)}\left[\tilde{P}_{n-1}^{(k+1)} + \tilde{P}_{n-3}^{(k+1)}\right] + c^{(k+1)}\left[\tilde{P}_n^{(k+1)} + \tilde{P}_{n-4}^{(k+1)}\right] + p_2^{(k+1)}\tilde{P}_{m_-}^{(k+1)} + 1.
\end{aligned} \tag{49}$$

These equations have *exactly* the desired form of the corresponding unrenormalized ones in equations (44), necessitating renomalization recursions for the parameters of the form

$$\begin{aligned}
a^{(k+1)} &= \frac{\left[a^{(k)}b^{(k)} + c^{(k)}\left(1 - p_1^{(k)}\right)\right]\left(1 + p_1^{(k)}\right)}{1 - \left(p_1^{(k)}\right)^2 - 2a^{(k)}b^{(k)}},\\
b^{(k+1)} &= \frac{a^{(k)}b^{(k)} + c^{(k)}\left(1 - p_1^{(k)}\right)}{1 - p_1^{(k)} - 2a^{(k)}b^{(k)}},\\
c^{(k+1)} &= \frac{a^{(k)}b^{(k)}p_1^{(k)}}{1 - \left(p_1^{(k)}\right)^2 - 2a^{(k)}b^{(k)}},\\
p_1^{(k+1)} &= \frac{p_2^{(k)}\left(1 - p_1^{(k)}\right)}{1 - p_1^{(k)} - 2a^{(k)}b^{(k)}},\\
p_2^{(k+1)} &= \frac{p_2^{(k)}\left[1 - \left(p_1^{(k)}\right)^2\right]}{1 - \left(p_1^{(k)}\right)^2 - 2a^{(k)}b^{(k)}}.
\end{aligned} \tag{50}$$

The analysis of the fixed points for $k \to \infty$ of equations (50) is surprisingly subtle. Of course, we obtain a rather simple fixed point for the choice of $p = 0$, which eliminates all long-range jumps. Then, $c^{(k)}$, $p_1^{(k)}$ and $p_2^{(k)}$ vanish for $k = 0$ in the initial conditions in (45) and remain zero for all $k > 0$, according to equations (50). As a consequence, the distinction between $a^{(k)}$ and $b^{(k)}$ disappears and both recursions reduce *exactly* to that for the unbiased one-dimensional walk in equation (27) with $a^* = b^* = \frac{1}{2}$, leading to ordinary diffusion with $d_w = 2$ and $\mu = \frac{3}{2}$, as discussed in section 4.1.1. Clearly, this fixed point is unstable with respect to variations in p.

For *any* probability $p > 0$ inserted into equations (45), the recursions in (50) evolve toward an apparent fixed point at $a^* = b^* = c^* = 0$ and $p_1^* = p_2^* = 1$. But these recursions are *singular* at such a fixed point, requiring a more detailed investigation. If we choose an arbitrarily small $\delta > 0$ and set $p = 1 - \delta$, we find that for all $k \geqslant 0$ it is $a^{(k)} \sim b^{(k)} \sim c^{(k)} = O(\delta)$ and $p_1^{(k)} \sim p_2^{(k)} = 1 - O(\delta)$. Hence, setting $\delta = 0$ in the end indeed validates this fixed point. Yet, the physics of this fixed point, corresponding to choosing $p = 1$, is trivial and does not reflect the numerical observations: strictly for $p = 1$ there is *no* transport at all along the backbone, and any walker is confined forever to jump back-and-forth on the first long-range link it accesses, which would imply $d_w = \infty$ in equation (17). For any choice of $0 < p < 1$, no matter how close to unity p gets, at long-enough times the walker 'escapes' along the backbone sufficiently often to explore ever-longer jumps both, to prevent confinement and to exceed ordinary diffusion. Thus, we must conclude that even this confinement fixed point is unstable and there has to be a third fixed point, at least.

To find this fixed point, we have to move beyond looking at the stationary behavior ($k = \infty$) of equations (50). Although equations (50) represent a five-dimensional parameter space, there do not appear to be any further stationary points reachable from the initial conditions in equations (45) aside from those two already discussed. As all flow appears to converge toward the singular confinement fixed point, we make an ansatz inserted into equations (50) for $k \gg 1$ that explores asymptotically the boundary layer [15] in its vicinity,

$$y^{(k)} \sim A_y \alpha^{-k} \qquad (y \in \{a, b, c, 1 - p_1, 1 - p_2\}), \tag{51}$$

with the assumption that $\alpha > 1$. Expanding equations (50) to leading order in α^{-k}, we find an over-determined system of equations

$$\begin{aligned}
\frac{1}{\alpha}A_a &= \frac{1}{\alpha}A_b = \frac{A_a^2}{A_{1-p_1}} + A_c,\\
\frac{1}{\alpha}A_c &= \frac{A_a^2}{2A_{1-p_1}},\\
\frac{1}{\alpha}A_{1-p_1} &= A_{1-p_2} - \frac{2A_a^2}{A_{1-p_1}},\\
\frac{1}{\alpha}A_{1-p_2} &= A_{1-p_1} - \frac{A_a^2}{A_{1-p_1}}.
\end{aligned} \tag{52}$$

Exercising the freedom to choose $A_a = 1$, we find

$$A_b = A_a = 1, \qquad A_c = \frac{1}{2\phi}, \qquad A_{1-p_1} = 2, \qquad A_{1-p_2} = \phi^2, \tag{53}$$

where

$$\phi = \frac{\sqrt{5}+1}{2} = 1.6180\ldots \tag{54}$$

is the 'golden ratio' [16], and obtain the eigenvalue equation

$$\alpha^3(\alpha+3) = 8. \tag{55}$$

It has a unique solution that satisfies the condition on the boundary layer, $\alpha > 1$, namely

$$\alpha = \frac{2}{\phi} = 1.2361\ldots. \tag{56}$$

Thus, we found another fixed point, lurking in the boundary layer of the confinement fixed point but with very distinct physical properties from it. Each reduction of the system size by a factor of 2 is accompanied by a rescaling of the hopping parameters by a factor of α^{-1}, bringing them closer to confinement, yet, leaving just enough room to escape and find still longer jumps. In fact, at this point of the analysis it is not even obvious whether these ever less frequent escapes from total confinement ultimately would result in sub-diffusive, normal or super-diffusive behavior.

The leading-order ansatz in equation (51) merely provided the existence of a third fixed point at infinite times. Extending the analysis to include finite-time corrections (i.e., $\epsilon = 1 - z \ll 1$), we include first-order corrections,

$$y^{(k)} \sim A_y \alpha^{-k}\{1 + \epsilon B_y \beta^k + \cdots\}, \tag{57}$$

expand the recursions in (50) in ϵ, and then also use the fact that α^{-k} is small. Using the leading-order constants A_y in equations (53), also the next-leading constants B_y are determined self-consistently. We extract, again uniquely,

$$\beta = 2\alpha = \frac{4}{\phi} \tag{58}$$

and find, choosing $B_a = 1$,

$$B_b = B_a = 1, \qquad B_c = \frac{4}{5}\phi, \qquad B_{1-p_1} = -\frac{6}{5}, \qquad B_{1-p_2} = -\frac{8}{5\phi^2}. \tag{59}$$

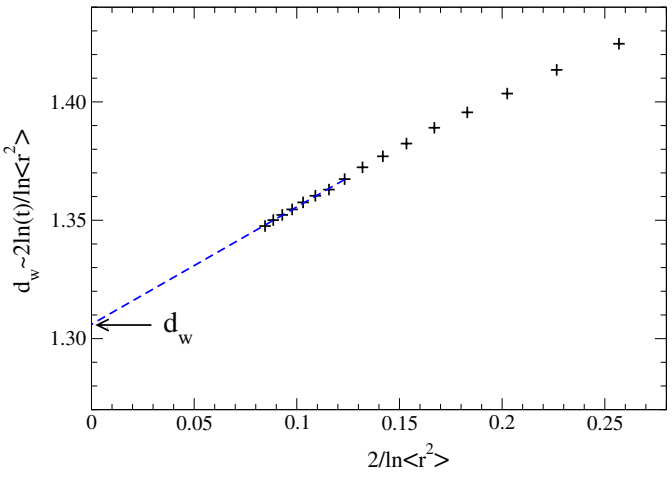

Figure 10. Plot of the results from simulations of the mean-square displacement of random walks on HN3 displayed in figure 1. More than 10^7 walks were evolved up to $t_{\max} = 10^6$ steps to measure $\langle r^2 \rangle_t$. The data are extrapolated according to equation (17), such that the intercept on the vertical axis determines d_w asymptotically. The exact result from equation (61) is indicated by the arrow.

Accordingly, time rescales as

$$T \to T' = \frac{4}{\phi} T, \tag{60}$$

and we obtain from equation (17) with $T \sim L^{d_w}$ for the diffusion exponent for HN3,

$$d_w = 2 - \log_2 \phi = 1.305\,76\ldots. \tag{61}$$

Our simulations in figure 10 are in excellent agreement with this result for d_w.

To extract the scaling behavior of the first-return distribution $Q_0(t)$ defined in equation (35), we proceed similar to the discussion in section 4.1.1. Here, we will find that different sites behave differently with respect to their return-time behavior, which is not surprising as the hierarchy of long-range jumps restricts translational invariance along the backbone. As in the discussion of first returns in section 4.1.1, we anticipate that we need an expansion of the parameters to order ϵ^2, i.e., we extend the ansatz in equation (57) even further. We find that it is sufficient to use

$$\begin{aligned} y^{(k)} &\sim A_y \alpha^{-k} \left\{ 1 + \epsilon B_y \beta^k + \epsilon^2 C_y \beta^{2k} + \cdots \right\} \\ &\sim A_y \left\{ \alpha^{-k} + \epsilon B_y 2^k + \epsilon^2 C_y (4\alpha)^k + \cdots \right\} \end{aligned} \tag{62}$$

with

$$\begin{aligned} C_a = C_b &= \frac{121}{25}\frac{\phi}{16}, & C_c &= \frac{121}{25}\frac{\phi^2}{16}, \\ C_{1-p_1} &= -\frac{121}{25}\frac{\phi}{16}, & C_{1-p_2} &= -\frac{121}{25}\frac{1}{16\phi} \end{aligned} \tag{63}$$

where we have also dropped at each order in ϵ terms that grow less than the leading exponential in k. For the coefficients C_y there is no freedom to choose, as they are a result of quadratic terms of the previous order, $\epsilon B_y \beta^k$; other terms with that freedom are subdominant.

As for equation (30), after $k = K - 1$ RG steps, the system has reduced to an elementary graph consisting of a single segment like that one shown in figure 9 (left) with $n = 2$ but with

$p_2 = 0$. Now, all even sites ($l = 0, 2, 4$) are no longer connected to a long-range jump. (Jumps of rate c do not count as long-range, since $c \to 0$ for $k \to \infty$, whereas $p_1 \sim p_2 \to 1$.) We therefore consider two (extreme) possibilities: (1) returns to a starting point at the boundary ($l = 0, N$) or central site ($l = N/2$) on the network and (2) returns to a site ($l = N/4$ or $l = 3N/4$) with the longest-possible long-range jump on the original network.

First, we consider case (1) of starting at a boundary site, say, $l = 0$. It is easy to show that the central site $l = N/2$ behaves identical to those on the boundary, and furthermore, even making the boundary sites more accessible be using periodic boundary conditions does not change the conclusion. We solve the system of equations

$$\begin{aligned}
\tilde{P}_0 &= a\tilde{P}_1 + c\tilde{P}_2 + 1,\\
\tilde{P}_1 &= 2b\tilde{P}_0 + b\tilde{P}_2 + p_1\tilde{P}_3,\\
\tilde{P}_2 &= a[\tilde{P}_1 + \tilde{P}_3] + 2c[\tilde{P}_0 + \tilde{P}_4],\\
\tilde{P}_3 &= b\tilde{P}_2 + 2b\tilde{P}_4 + p_1\tilde{P}_1,\\
\tilde{P}_4 &= a\tilde{P}_3 + c\tilde{P}_2,
\end{aligned} \tag{64}$$

where we have suppressed the superscript $(K-1)$ on the generating function and the parameters alike. (As we have learned from the 1D-walk in equation (30), the hopping parameters originating from the boundary sites $l = 0$ and $l = 4$ have to be doubled due to the reflecting boundaries.) The solution for $\tilde{P}_0$ of this system of equations yields

$$\tilde{P}_0 = \frac{(1-2c^2)\left(1-p_1^2\right) - 2ab[1+(1+2c)(1+p_1)] + 2a^2b^2}{[(1-p_1)(1-2c) - 4ab](1+2c)(1+p_1-2ab)}. \tag{65}$$

Note that *both,* numerator and denominator, decay asymptotically like $\sim 1 - p_1^2$ near the stable fixed point. Dividing out that behavior, both behave as $1 + y^{(K)}$ with $y^{(K)}$ as in equation (62), where y here stands for a mix of coefficient that results from multiplying out the terms in numerator and denominator, respectively. Since we do not expect any spurious cancellations, the ratio of these two expressions *also* results in the form $1 + y^{(K)}$. Hence, making superscripts reappear, we find from equation (62)

$$\frac{1}{\tilde{P}_0^{(K-1)}} \sim 1 + \mathcal{B}\epsilon 2^K + \mathcal{C}\epsilon^2(4\alpha)^K + \cdots, \tag{66}$$

where we have also dropped the α^{-K}-term in order ϵ^0 and marked constants that are unimportant for the scaling with K by calligraphy script. Solving the recursions in equation (47) for $l = 0$ and inserting the solution into the relation for $\tilde{Q}_0$ in equation (33), we find

$$\begin{aligned}
\tilde{Q}_0 &= 1 - \frac{1}{\tilde{P}_0^{(0)}}\\
&= 1 - \frac{1}{\tilde{P}_0^{(K-1)}} \prod_{k=0}^{K-2}\left[1 - \frac{2a^{(k)}b^{(k)}}{1-\left(p_1^{(k)}\right)^2}\right].
\end{aligned} \tag{67}$$

Ignoring at most a finite number of factors in the product (hence, missing an overall constant $\mathcal{A}$), we can expand the remaining factors in the product using the asymptotic expansion in equation (62) for $1 \ll k \leqslant K-2 \to \infty$,

$$\begin{aligned}
\prod_{k=0}^{K-2}\left[1 - \frac{2a^{(k)}b^{(k)}}{1-\left(p_1^{(k)}\right)^2}\right] &\sim \mathcal{A}\prod_{k\gg 1}^{K-2}[1 - \alpha^{-k} + \mathcal{D}\epsilon 2^k + \mathcal{E}\epsilon^2\,(4\alpha)^k + \cdots],\\
&\sim \mathcal{A}\left[1 - \mathcal{D}\epsilon\sum_{k\gg 1}^{K-2} 2^k + \mathcal{E}\epsilon^2\sum_{k\gg 1}^{K-2}(4\alpha)^k + \cdots\right],\\
&\sim \mathcal{A} + \mathcal{F}\epsilon 2^K + \mathcal{G}\epsilon^2(4\alpha)^K + \cdots.
\end{aligned} \tag{68}$$

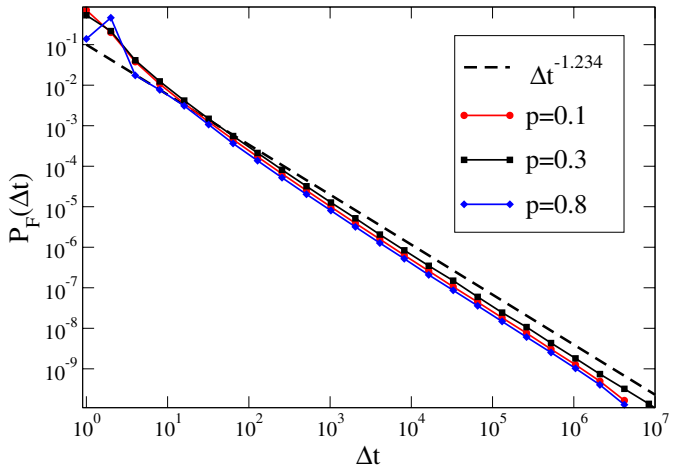

Figure 11. Plot of the probability $Q(\Delta t)$ of first returns to the origin after Δt update steps on a system of unlimited size. Data were collected for three different walks on HN3 with $p = 0.1$ (circles), $p = 0.3$ (squares) and $p = 0.8$ (diamonds). The data with the smallest and largest p exhibit strong transient effects. The exact result in equation (70), $\mu = 1.234\ldots$, is indicated by the dashed line.

Note that $0 < \mathcal{A} < 1$, as each factor in the product must be between $\frac{1}{2}$ and 1 for any choice the probability p. Inserting equations (66) and (68) into equation (67), we obtain

$$\tilde{Q}_0 \sim (1 - \mathcal{A}) + \mathcal{H}\epsilon 2^K + \mathcal{I}\epsilon^2 (4\alpha)^K + \cdots. \tag{69}$$

This result implies first that returns to sites like $l = 0, N/2, N$ are *not* recurrent because walks may escape forever with a finite probability $\mathcal{A}$. Finally, an application of equation (40) produces

$$\langle t \rangle_K \sim 2^K \sim N, \qquad \langle t^2 \rangle_K \sim (4\alpha)^K \sim N^{\log_2(4\alpha)},$$

hence, with equation (38) and $\alpha = 2/\phi$,

$$\mu = 2 - \frac{1}{2 - \log_2(\phi)} = 1.234\,16\ldots. \tag{70}$$

A relation of this form, $\mu = 2 - 1/d_w$, is commonly found for Lévy flights [17], and the result is again borne out by our simulations, see figure 11.

Case (2), referring to walkers starting near the longest jump in the network, is represented by the system

$$\begin{aligned}
\tilde{P}_0 &= a\tilde{P}_1 + c\tilde{P}_2, \\
\tilde{P}_1 &= 2b\tilde{P}_0 + b\tilde{P}_2 + p_1\tilde{P}_3 + 1, \\
\tilde{P}_2 &= a[\tilde{P}_1 + \tilde{P}_3] + 2c[\tilde{P}_0 + \tilde{P}_4], \\
\tilde{P}_3 &= b\tilde{P}_2 + 2b\tilde{P}_4 + p_1\tilde{P}_1, \\
\tilde{P}_4 &= a\tilde{P}_3 + c\tilde{P}_2,
\end{aligned} \tag{71}$$

with the constant term from the initial conditions now near an odd site, say, $l = 1$. Solving for the launch site of the walk, we find

$$\tilde{P}_1 = \frac{1 - 2c - ab(3 - 2c)}{[(1 - p_1)(1 - 2c) - 4ab](1 + p_1 - 2ab)}. \tag{72}$$

Note that in this case *only* the denominator of $\tilde{P}_1 = \tilde{P}_1^{(K-1)}$ decays with $1-p_1$ on approaching the stable fixed point which will ensure that $\tilde{P}^{(0)}_{N/4}$ diverges, making this process recurrent on behalf of equation (33). In contrast to equation (66), we find here

$$\begin{aligned}\frac{1}{\tilde{P}_1^{(K-1)}} &\sim (1-p_1)[1+\mathcal{J}\epsilon 2^K + \mathcal{K}\epsilon^2(4\alpha)^K + \cdots],\\ &\sim A_{1-p_1}\alpha^{-K+1}[1+\mathcal{J}\epsilon 2^K + \mathcal{K}\epsilon^2(4\alpha)^K + \cdots]\\ &\quad\times[1+\epsilon B_{1-p_1}(2\alpha)^{K-1} + \epsilon^2 C_{1-p_1}(2\alpha)^{2K-2} + \cdots],\\ &\sim (2\alpha)\alpha^{-K}[1+\mathcal{L}\epsilon(2\alpha)^K + \mathcal{M}\epsilon^2(2\alpha)^{2K} + \cdots],\end{aligned} \tag{73}$$

where the last step is justified by the observation that the leading terms order by order in ϵ in the first square bracket dominate over those in the second.

We have to solve the recursions in equation (48) for this case to obtain

$$\tilde{P}^{(0)}_{\frac{N}{4}} = \tilde{P}_1^{(K-1)} \prod_{k=0}^{K-2} \frac{1-p_1^{(k)}}{1-p_1^{(k)} - 2a^{(k)}b^{(k)}}$$

and from equation (33),

$$\begin{aligned}\tilde{Q}_{\frac{N}{4}} &= 1 - \frac{1}{\tilde{P}^{(0)}_{\frac{N}{4}}},\\ &= 1 - \frac{1}{\tilde{P}_1^{(K-1)}} \prod_{k=0}^{K-2}\left[1 - \frac{2a^{(k)}b^{(k)}}{1-p_1^{(k)}}\right].\end{aligned} \tag{74}$$

The product in equation (74) behaves identically to that discussed above in equation (68) and hence will not alter the overall form of the expansion when multiplying $1/\tilde{P}_1^{(K-1)}$ in equation (73). Then we get

$$\begin{aligned}\tilde{Q}_{\frac{N}{4}} &\sim 1 - (2\alpha)\alpha^{-K}[1+\mathcal{N}\epsilon(2\alpha)^K + \mathcal{O}\epsilon^2(2\alpha)^{2K} + \cdots],\\ &\sim 1 - (2\alpha)\alpha^{-K} + \mathcal{P}\epsilon 2^K + \mathcal{Q}\epsilon^2(4\alpha)^K + \cdots.\end{aligned} \tag{75}$$

This result is almost identical to that for returns to the origin above in equation (69), except that sites at the longest jump in the system are recurrent, i.e., $\tilde{Q}_{N/4} \equiv 1$ for large systems ($K \to \infty$) and times ($\epsilon = 1 - z \to 0$). (Presumably recurrence will gradually degrade from the strictly recurrent sites at the highest level in the hierarchy to those at the lowest.) Yet, the scaling of return times in form of the exponent μ is described by equation (70) for *all* sites.

4.2. Generating function for random walks on HN4

Next, we consider a random walk on HN4. The 'master equation' [14] for the probability of the walker to be at site n, as defined in equation (1), at time t is given by

$$P_{n,t} = \frac{1-p}{2}[P_{n-1,t-1} + P_{n+1,t-1}] + \frac{p}{2}[P_{n-2^{i+1},t-1} + P_{n+2^{i+1},t-1}], \tag{76}$$

where p is the probability to make a long-range jump. (Throughout, we considered p uniform, independent of n or t). To make the connection between n and i explicit, we rewrite equation (76) as

$$\begin{aligned}P_{2^i(2j+1),t} &= \frac{1-p}{2}[P_{2^i(2j+1)-1,t-1} + P_{2^i(2j+1)+1,t-1}] + \frac{p}{2}[P_{2^i(2j-1),t-1} + P_{2^i(2j+3),t-1}],\\ P_{0,t} &= \frac{1-p}{2}[P_{-1,t-1} + P_{1,t-1}] + pP_{0,t-1}.\end{aligned} \tag{77}$$

Note that the case $n = 0$ is not covered by equation (1) and, hence, must be treated separately. Here, we choose the site $n = 0$ to be the only one connected to itself such that HN4 is 4-regular throughout, as depicted in figure 2.

It is straightforward to apply the generating function in equation (20) again, assuming, for simplicity, the initial condition

$$P_{n,0} = \delta_{n,0}. \tag{78}$$

We obtain

$$\begin{aligned} \tilde{P}_{2^i(2j+1)} &= \frac{1-p}{2} z[\tilde{P}_{2^i(2j+1)-1} + \tilde{P}_{2^i(2j+1)+1}] + \frac{p}{2} z[\tilde{P}_{2^i(2j-1)} + \tilde{P}_{2^i(2j+3)}], \\ \tilde{P}_0 - 1 &= \frac{1-p}{2} z[\tilde{P}_{-1} + \tilde{P}_{1,}] + pz\tilde{P}_0. \end{aligned} \tag{79}$$

While the overall structure of this problem is even more symmetric than for HN3 in section 4.1.2, a RG treatment does not seem possible in this case. Tracing out all odd sites would immediately interconnect *all* other remaining sites. (The resulting infinite set of coupled equations may have certain symmetry properties that would lend themselves for a recursive treatment. We have not yet explored such a possibility.)

In contrast to an ordinary lattice, say, it is also not straightforward to solve this equation by a Fourier transform such as

$$F(z, \phi) = \sum_{n=-\infty}^{\infty} \tilde{P}_n(x)\, \mathrm{e}^{n\phi I}, \tag{80}$$

defining $I = \sqrt{-1}$. Considering the $1 - p$-terms, originating from nearest-neighbor jumps, and the p-terms, originating from long-range jumps, in equations (79) separately provides for regularly-spaced patterns, level by level in the hierarchy. But the mixing of nearest-neighbor and long-range jumps destroys this regularity. Hence, we resort to transforming equations (79) in each level i with a partial transform,

$$\Pi_i(z, \phi) = \sum_{j=-\infty}^{\infty} \tilde{P}_{2^i(2j+1)}(z) \exp\{2^i(2j+1)\phi I\}. \tag{81}$$

Inserting equation (81) and application of the general theorem

$$\sum_{i=1}^{\infty} \sum_{j=-\infty}^{\infty} f_{2^i(2j+1)\pm 1} = \sum_{j=-\infty}^{\infty} f_{2j+1} - f_{\pm 1}, \tag{82}$$

which results because $2^i(2j+1)$ for $i \geqslant 1$ exactly runs over all even numbers $\neq 0$ and over all odd numbers for $i = 0$, yields for equations (79),

$$\begin{aligned} \sum_{i=1}^{\infty} \Pi_i[1 - pz\cos(2^{i+1}\phi)] &= (1-p)z\cos\phi\,\Pi_0 + 1 - (1-pz)\tilde{P}_0, \\ \Pi_0[1 - pz\cos(2\phi)] &= (1-p)z\cos\phi \sum_{i=1}^{\infty} \Pi_i + (1-p)z\cos\phi\,\tilde{P}_0. \end{aligned} \tag{83}$$

We can combine both relations to get

$$1 = [1 - zp - (1-p)z\cos\phi]F + zp \sum_{i=0}^{\infty} [1 - \cos(2^{i+1}\phi)]\Pi_i, \tag{84}$$

using equations (80) and (81) to eliminate $\tilde{P}_0$ via

$$\sum_{i=0}^{\infty} \Pi_i = \sum_{i=0}^{\infty} \sum_{j=-\infty}^{\infty} \tilde{P}_{2^i(2j+1)} \exp\{2^i(2j+1)\phi I\},$$
$$= \sum_{n=-\infty}^{\infty} \tilde{P}_n e^{n\phi I} - \tilde{P}_0,$$
$$= F - \tilde{P}_0. \tag{85}$$

At this point, there does not seem to be any further progress possible on equation (84), due to the term $\sum_i \Pi_i \cos(2^{i+1}\phi)$, which resembles a Weierstrass function [18]. At best, on could try to extract information about the moments of the walk,

$$\langle n^k \rangle_t = \sum_{n=-\infty}^{\infty} n^k P_{n,t},$$

via the moment-generating function

$$M_k(z) = \sum_{t=0}^{\infty} \langle n^k \rangle_t z^t,$$
$$= [-I\partial_\phi]^k F(z,\phi)|_{\phi=0}. \tag{86}$$

Note that the second moment $M_2(z)$ already would provide the exponent d_w on behalf of the definition in equation (17). (All odd moments vanish, of course, as equation (84) is even in ϕ.) The zeroth moment, setting $\phi = 0$ in equation (84), simply results in

$$M_0(z) = \frac{1}{1-z},$$

which just demonstrates that everything is properly normalized, $\mathcal{N}_t = \langle n^0 \rangle_t = \sum_{n=-\infty}^{\infty} P_{n,t} = 1$, at all times t. But already the second moment would lead to terms containing $\sum_i \Pi_i 4^i$, which we cannot account for, even at $\phi = 0$ and in the limit $z \to 1^-$.

Instead, we note that the long-time behavior is dominated by the long-range jumps, as discussed for HN3 in section 4.1.2. To simplify matters, we set $p = 1/2$ here, although any finite probability would lead to the same conclusions. We make an 'annealed' approximation, i.e., we assume that we happen to be at some site n in equation (1) with probability $1/2^i$, corresponding to the relative frequency of such a site, yet independent of time or history. This ignores the fact that in the network geometry a long jump of length 2^i can be followed *only* by another jump of that length or a jump of unit length, and that many intervening steps are necessary to make a jump of length 2^{i+1}, for instance. Here, at each instant the walker jumps a distance 2^i left or right irrespectively with probability $1/2^{i+1}$, and we can write

$$\mathcal{P}_{n,t} = \sum_{n'} T_{n,n'} \mathcal{P}_{n',t-1} \tag{87}$$

with

$$T_{n,n'} = \frac{a-1}{2a} \sum_{i=0}^{\infty} a^{-i} (\delta_{n-n',b^i} + \delta_{n-n',-b^i}), \tag{88}$$

where $a = b = 2$. Equations (87)–(88) are identical to the Weierstrass random walk discussed in [18, 19] for arbitrary $1 < a < b^2$. There, it was shown that $d_w = \ln(a)/\ln(b)$, which leads to the conclusion that $d_w = 1$ in equation (17) for HN4, as has been predicted (with logarithmic corrections) on the basis of numerical simulations in [11].

5. Conclusions

We have shown how the powerful tools of the dynamic renormalization group [14] allow us to dissect this intricate random walk problem on the planar network HN3 with a 'hidden' fixed point. Indeed, using a boundary-layer analysis, we unravel the irregular singularity of the dominant fixed point in a five-dimensional parameter space, resulting in a set of exact, non-trivial exponents describing super-diffusive transport. Adding just one more link to each site, we obtain a non-planar network HN4 which possess an even higher degree of symmetry, yet, for which we can only develop an equation for the generator and an alternative 'annealed' treatment which provides results that are consistent with simulations. (We believe that a proper exploitation of the symmetry in HN4, which eludes us here, will ultimately make exact results possible.)

Aside from the singular fixed point, HN3 serves further as an instructive example for a network in which nodes have heterogeneous recurrence properties. The diffusion exponent d_w is larger than the fractal dimension $d_f = 1$ of the lattice backbone that the walk is embedded in, which usually implies recurrence [20, 21]. Here, the near-confined state of the walk favors recurrences to sites in higher levels of the hierarchy, although the associated first-return exponent is the same for all sites for the time distribution of any given return.

We should also mention that our results for HN3 can have an alternative interpretation. If we ignore the one-dimensional lattice backbone and instead consider the network as a graph without particular embedding, then equation (4) for the diameter, or more specifically the average growth in neighborhood $S_d \sim d^2$ with jump distance d found in figure 6, implies that the fractal dimension for that graph is $d_f = 2$. The RG would discover the then-obscured asymmetry between the backbone and long-range jumps (even when starting with $p = 1/3$) and lead to the same analysis. Yet, with all distances now being (on average) measured as the square root of their separation along the backbone, also the mean-square displacement in equation (17) needs to be re-evaluated, yielding a diffusion exponent twice its previous value, $d_w = 2(2 - \log_2 \phi) = 2.61\ldots$. In this interpretation, $d_w > d_f$ still applies, but walks are now sub-diffusive in this metric. Of course, an exponent that is independent of such a metric, like the purely event-base first return probability, does *not* change. In turn, the relation between d_w and μ fails, consistent with the fact that the walk can no longer be considered a Lévy flight.

Finally, our results suggest that many other interesting transport phenomena, such as voter models, exclusion processes or self-organized critical phenomena can be fruitfully studied on these networks, which are sufficiently complex for interesting results but sufficiently simple to be tractable. Especially in light of the tremendous interest in complex dynamics on designed structures, we hope that these networks can make a useful contribution [7–9, 22].

References

[1] Erdös P and Rényi A 1973 *The Art of Counting* (Cambridge, MA: MIT Press)
[2] Bollobas B 1985 *Random Graphs* (London: Academic)
[3] Berker A N and Ostlund S 1979 *J. Phys. C: Solid State Phys.* **12** 4961
[4] Migdal A A 1976 *J. Exp. Theor. Phys.* **42** 743
[5] Kadanoff L P 1976 *Ann. Phys.* **100** 359
[6] Mandelbrot B B 1982 *The Fractal Geometry of Nature* (San Francisco: Freeman)
[7] Barabasi A-L, Ravasz E and Vicsek T 2001 *Physica* A **299** 559
[8] Andrade J S, Herrmann H-J, Andrade R F S and da Silva L R 2005 *Phys. Rev. Lett.* **94** 018702
[9] Zhang Z, Zhou S, Fang L, Guan J and Zhang Y 2007 *Europhys. Lett.* **79** 38007
[10] Southern B W and Young A P 1977 *J. Phys. C: Solid State Phys.* **10** 2179
[11] Boettcher S, Gonçalves B and Guclu H 2007 *J. Phys. A: Math. Theor.* **41** 252001

[12] Boettcher S and Gonçalves B 2008 *Preprint* arXiv:0802.2757
[13] Watts D J and Strogatz S H 1998 *Nature* **393** 440
[14] Redner S 2001 *A Guide to First-Passage Processes* (Cambridge: Cambridge University Press)
[15] Bender C M and Orszag S A 1978 *Advanced Mathematical Methods for Scientists and Engineers* (New York: McGraw-Hill)
[16] Livio M 2003 *The Golden Ratio: The Story of PHI, the World's Most Astonishing Number* (New York: Broadway Books)
[17] Metzler R and Klafter J 2004 *J. Phys. A: Math. Gen.* **37** R161
[18] Hughes B D, Shlesinger M F and Montroll E W 1981 *Proc. Natl. Acad. Sci.* **78** 3287
[19] Shlesinger M F, Zaslavsky G M and Klafter J 1993 *Nature* **363** 31
[20] Bollt E M and Avraham D ben 2005 *New J. Phys.* **7** 26
[21] Condamin S, Benichou O, Tejedor V, Voituriez R and Klafter J 2007 *Nature* **450** 77
[22] Hinczewski M and Berker A 2006 *Phys. Rev.* E **73** 066126